Dieses Dokument ist eine Zweitveröffentlichung (Verlagsversion) /

This is a self-archiving document (published version):

M. Germer, U. Marschner, A. B. Flatau

Design and experimental verification of an improved magnetostrictive energy harvester

Diese Version ist verfügbar / This version is available on:

https://nbn-resolving.org/urn:nbn:de:bsz:14-qucosa2-351349

PROCEEDINGS OF SPIE

Design and experimental verification of an improved magnetostrictive energy harvester

M. Germer, U. Marschner, A. B. Flatau

SPIE.

Design and Experimental Verification of an Improved Magnetostrictive Energy Harvester

M. Germer[a], U. Marschner[a], and A.B. Flatau[b]

[a]Institute for Semiconductor and Microsystems Technology, Technical University of Dresden, 01062 Dresden, Germany
[b]University of Maryland, Department of Aerospace Engineering, College Park, MD, USA

ABSTRACT

This paper summarizes and extends the modeling state of the art of magnetostrictive energy harvesters with a focus on the pick-up coil design. The harvester is a one-sided clamped galfenol unimorph loaded with two brass pieces each containing a permanent magnet to create a biased magnetic field. Measurements on different pick-up coils were conducted and compared with results from an analytic model. Resistance, mass and inductance were formulated and proved by measurements. Both the length for a constant number of turns and the number of turns for a constant coil length were also modeled and varied. The results confirm that the output voltage depends on the coil length for a constant number of turns and is higher for smaller coils. In contrast to a uniform magnetic field, the maximal output voltage is gained if the coil is placed not directly at but near the fixation. Two effects explain this behavior: Due to the permanent magnet next to the fixation, the magnetic force is higher and orientates the magnetic domains stronger. The clamping locally increases the stress and forces the magnetic domains to orientate, too. For that reason the material is stiffer and therefore the strain smaller. The tradeoff between a higher induced voltage in the coil and an increasing inductance and resistance for every additional turn are presented together with an experimental validation of the models. Based on the results guidelines are given to design an optimal coil which maximizes the output power for a given unimorph.

Keywords: Magnetostrictive energy harvester, Solenoid coil optimization, Coil position

1. INTRODUCTION

Vibrational energy harvesting is a promising method for wireless applications for which it is difficult and time-consuming to regularly replace the battery as traditional energy source. Especially in harsh environments and with the upcoming amount of sensors the disadvantage of the lifetime limiting battery needs to be circumvented. Vibrational piezoelectric single beam energy harvesters have been widely studied as continous energy supply. Depending on the material, they have either a high coupling factor but are extremely brittle or they are flexible but have a low energy conversion factor.[1] Moreover, they depolarize and have a limited lifetime.[2] Low and moderate Curie temperatures confines the field of application and is the reason why piezoelectrical energy harvesting is still critical.[3] In contrast to piezoelectric materials, another group of smart materials, so called magnetostrictive materials, such as galfenol (The group of iron-gallium alloys with $Fe_{100-x}Ga_x$ and $12 < x < 30$ is designated as galfenol.[4]), circumvents these disadvantages which makes them more interesting for extreme environmental conditions. Magnetostrictive materials exhibit a change in magnetic flux whenever a stress or strain is applied. In combination with a coil, the change of magnetic flux corresponding to Faraday's law induces a voltage in the coil and makes magnetostriction feasible for energy harvesting. Until today, only a few energy harvesters based on magnetostriction have been investigated. They all have in common, that a strain or stress is applied to the magnetostrictive material which consequently changes its magnetic flux density and induces a voltage in a closely wound coil. Wang and Yuan (2008) studied a system where a fixed-free end unimorph beam was surrounded by a coil. The unimorph consisted of a 0.4 mm thick copper support layer on which an eight-layered Metglas 2605SC (Metglas 2605SC is designated an amorphous metallic glass with $Fe_{81}B_{13.5}Si_{3.5}C_2$.) with a total active material volume of $0.95\,cm^3$ was bonded. Instead of using biasing magnets, they annealed Metglas beforehand under a strong transverse magnetic field, also known as field annealing. For the developed prototype they measured a maximal power of $576\,\mu W$ at a resonance frequency of $1.1\,kHz$ and a peak acceleration of $0.82\,g$. Furthermore, they deduced a model for the electromechanical coupling coefficient and concluded that the number of turns of

a coil does not influence the transducing process as long as the coil is long enough and can be treated as a long solenoid.[2]

Ueno and Yamada presented a system in 2011, in which two galfenol rods each measuring 1 mm x 0.5 mm x 10 mm are connected to a fixture and mover and surrounded by a coil. Two permanent magnets and a back iron yoke were attached to the structure to provide a biasing magnetic field for a better energy transduction. At a maximal displacement of 0.65 mm, this small system reached a peak output power of 2 mW at a resonance frequency of 395 Hz, using a wire of 0.05 mm, turned 312 times with a resistance of 15 Ω. Furthermore, they studied a setup where a mass was added to the mover and decreased the frequency to 94 Hz. During free vibration testing the authors observed, that the setup without additional mass returns a higher output energy for the same input energy.[5]

In 2012, Yoo and Flatau presented their concept of a magnetostrictive unimorph energy harvester. As depicted in Figure 1, they bonded a 50.8 mm x 6.4 mm x 0.8 mm long polycrystalline galfenol strip to an aluminum cantilever beam with a dimension of 50.8 mm x 6.4 mm x 1.3 mm. At both ends permanent magnets were mounted and fixed with brass pieces to create a bias magnetic field and to load additional mass on the beam. For their device, they measured an effective output power of 2.2 mW at a frequency of 222 Hz and
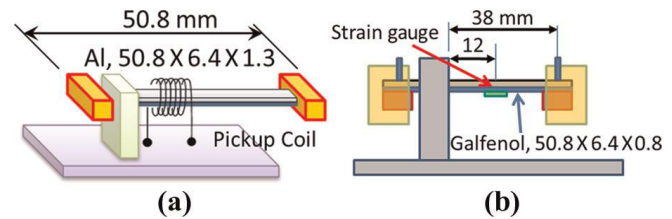
Figure 1: Galfenol unimorph energy harvester studied by Yoo and Flatau (2012):(a) isoview and (b) side view[4]

1 g base excitation. Based on classical equations Yoo and Flatau calculated the base excitation of a cantilever and modeled the output voltage using linearized piezomagnetic transduction equations and Faraday's law.[4]

Three years later, Ueno et al. improved the force factor for magnetostrictive energy harvesters[6] and Ueno analyzed and developed a sophisticated mechanical structure in which he focused on an amplified and more homogeneous compression and tension over the whole beam due to the fact that a simple fixed-free end beam has an inhomgeneous strain profile over its length. He reduced the size of galfenol to 2 mm x 0.5 mm x 7 mm and extended the number of turns to 1740. The wire had a diameter of 0.05 mm, resulting in a resistance of 120 Ω. Under a resonant vibration of 212 Hz and an excitation of 1.2 g the effective open-circuit voltage was measured 1.3 V and the maximal output power was gauged 1.2 mW.[7]

Most studies end up at the point, where a harvester is built and compared with a developed model without any further detailed parameter studies and optimization. In order to improve magnetostrictive energy harvesting and expand its promising potential, this work dedicates on parameter studies of a simple magnetostrictive energy harvester. Special attention is given to the coil as one of two main parts of the transduction mechanism. This work builds upon the work established by Yoo and Flatau in 2012 with some minor changes. The easy change of the pickup coil, the magnetostrictive unimorph, the beam length and the biasing magnet field makes the author's system most suitable for intense studies.

2. PHYSICAL BACKGROUND

2.1 Mechanial Lumped Element Modeling

The energy harvester with mass and cantilever can be reduced to a linear system as illustrated in Figure 2, consisting of three main elements: a mass, a stiffness and a damping. For such a system, the performance and the energy conversion strongly depend on the frequency. The maximum conversion occurs if the resonance frequency of the harvester coincides with the frequency of the system on which it is mounted. Therefore a model is presented, predicting the eigenfrequencies. Here, all investigations are taken with respect to the first eigenfrequency. The equation of motion of such a system for free vibrations is given by:

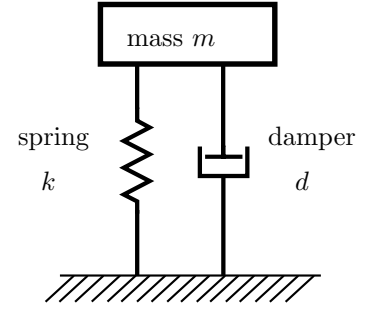$$m\ddot{z} + d\dot{z} + kz = 0 \tag{1}$$

where m is the mass of the system, d the damping coefficient and k the spring constant. This second order differential equation is solved, using the function $z = Ze^{\lambda t}$. Replacing z and rearranging the term leads to:

$$\lambda^2 + \underbrace{\frac{d}{m}}_{2\delta}\lambda + \underbrace{\frac{k}{m}}_{\omega_0^2} = 0 \tag{2}$$

$$\lambda_{1,2} = -\delta \pm \underbrace{\sqrt{\delta^2 - \omega_0^2}}_{\omega_d} \tag{3}$$

Figure 2: Lumped element model of a mass-, spring-, damper system

where ω_d is the angular frequency and δ is the damping constant. For systems where $\delta^2 << \omega_0^2$, it follows: $\omega_0 \approx \omega_d$. That is why $\omega_0 = \sqrt{k/m}$ is defined as resonance frequency of the system. Assuming that $\delta^2 << \omega_0^2$, leads to time-oscillating functions:

$$z = e^{-\delta t}[C_1 \cdot \cos(\omega_0 t) + C_2 \cdot \sin(\omega_0 t)] \tag{4}$$

where C_1 and C_2 are constants, determined by the initial condition. Equation 4 points a time-oscillating function with the frequency ω_0 and a decay of $e^{-\delta t}$. To calculate ω_0, it suffices to characterize the lumped elements spring and mass. The damping is necessary to specify the losses of the system. The following calculation for the lumped elements is based on the coordinate system as depicted in Figure 3. The beam is discretized in n equidistant mass elements m_i each with a length l/n and a mass m/n concentrated at the position x_i. Once, the system is excited, the beam oscillates with a certain frequency ω between the positions $z(l)$ and $-z(l)$ at the tip of the beam. Due to different deflections along the length, every single element of the beam moves with a different velocity $v_z(x_i)$ and depends on the frequency:

$$v_z(x_i) = z(x_i)\omega_0 \tag{5}$$

where $z(x_i)$ is the shape function.
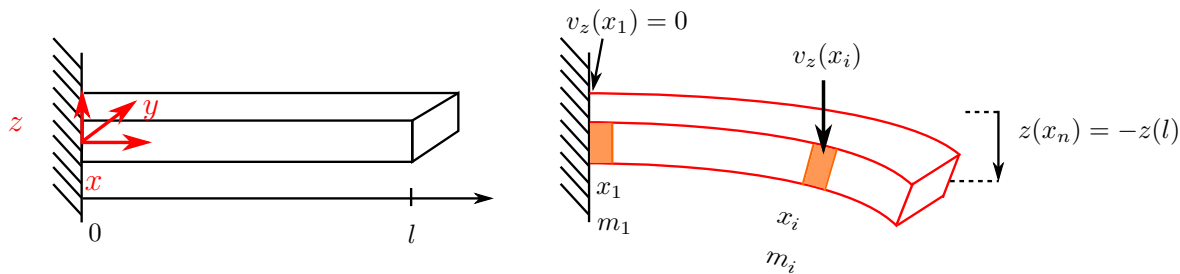
Figure 3: Coordinate system for a bended beam and its discretization into equidistant elements

2.1.1 Lumped Element - Mass

The lumped mass of the system contains all objects which move harmonically, namely beam, tip mass and in case that the coil is directly fixed on the beam, the coil as well. According to the position on the beam, the objects have different impacts. The effective mass, being the weighted sum of the contributing parts, is calculated by applying Rayleigh's energy method.[8] The maximal potential energy W_{max} is stored in the structure at maximum displacement.

$$W_{max} = \frac{1}{2}k_z[z(l)]^2 \tag{6}$$

where k_z is the spring constant. The total kinetic energy K_{max} equals the kinetic energy of the concentrated mass elements m_i with a velocity $v_z(x_i)$ along the length of the beam.

$$K_{max} = \frac{1}{2}\sum_{i=1}^{n} m_i[v_z(x_i)]^2 \tag{7}$$

applying the relation $v_z(x_i) = z(x_i)\omega_0$ and assuming that the potential energy is completely transferred into kinetic energy results in an expression for ω_0:

$$\omega_0 = \sqrt{\frac{k_z[z(l)]^2}{\sum_{i=1}^{n} m_i[z(x_i)]^2}} \qquad (8)$$

Comparing the coefficients from Equation 8 with $\omega_0 = \sqrt{k/m}$ allows to state the following relation for m and k:

$$k = k_z \qquad\qquad m = \frac{\sum_{i=1}^{n} m_i[z(x_i)]^2}{[z(l)]^2} \qquad (9)$$

The shape function can be deduced, using the Euler-Bernoulli beam theory, operating on the assumptions that planar cross sections remain planar and cross sections remain perpendicular to the deformed axis of the beam. The assumptions can be considered valid for small deflection for beams for which the dimension of length is dominant in comparison to the cross section. In case a force F at the tip end, directed along the negative z-axis, strains the clamped-free end cantilever, it can be shown, that the shape function $z(x)$ and the maximal deflection $z(l)$ are:[9]

$$z(x) = -\frac{F}{EI}\left(-\frac{x^3}{6} + \frac{lx^2}{2}\right) \qquad (10)$$

$$z(l) = -\frac{Fl^3}{3EI} \qquad (11)$$

where E is the Young's modulus and I is the area moment of inertia. For the selected coordinate system in this work, I is synonymously used as area moment of inertia I_y with respect to the y-axis. Taking into consideration that the harvester possesses two different metal layers with different Young's modulus and cross section, the product EI is generalized to the mean value $\overline{EI}$. By means of the shape function, the specific contribution to the lumped mass of each element can be calculated.

Tip mass
The tip mass is considered concentrated, located at the end of the beam and described by the δ-function.[10] As result, the entire tip mass $m_1 = m_{tip}$ contributes to the lumped mass.

$$m_1 = \frac{m_{tip}\int_{x=0}^{l}[z(x)]^2\delta(x-l)dx}{[z(l)]^2} \qquad (12)$$

Beam
To evaluate the contribution of the beam, the mass elements are considered infinitesimally small with a mass dm and a length dx. Replacing the sum by an integral with differential masses $dm = \rho_{beam}A_{beam}dx$ where ρ_{beam} and A_{beam} are density of the beam and cross section respectively, results in

$$m_2 = \frac{\int_{x=0}^{l}\rho_{beam}A_{beam}[z(x)]^2dx}{[z(l)]^2} \qquad (13)$$

Inserting Equation 10 and 11 into Equation 13 and solving the integral returns the effective mass of the beam $m_2 = 33/140\,m_{beam}$.

Coil
The coil covers the beam between $x = l_1$ and $x = l_2$. For homogeneously wound coils, it is assumed, that the distributed mass behaves like a concentrated mass at $l_{coil} = (l_2 - l_1)/2$. Analogous to the calculation of the effective mass of the tip mass, the contribution of the coil can be estimated in case the coil touches the beam:

$$m_3 = \frac{\int_{x=0}^{l}\rho_{coil}A_{coil}[z(x)]^2\delta(x-l_{coil})dx}{[z(l)]^2} \qquad (14)$$

Total mass

The lumped mass is easily calculated by the sum: $m = m_1 + m_2 + m_3$. In case, that the coil does not touch the beam, it has no influence and the lumped mass equals $m = m_{tip} + 33/140 \, m_{beam}$.

2.1.2 Lumped Element - Spring

The spring is mainly given by the geometry and the mechanical properties of the beam. Nevertheless, a tightly mounted coil also influences the stiffness and depends on the force with which the coil is clamped on the beam. To predict the total influence, a large series of estimations for different coils would be necessary but even then the approximations would be valid only for the studied unimorph and one type of coils. As it will be shown later in Section 5, coils which do not touch the beam are advantageous and circumvent this issue. For these coils, only the stiffness of a fixed - free end two-layer beam is relevant and described by:

$$k = \frac{3\overline{EI}}{l^3} \tag{15}$$

The bending stiffness is the product of Young's modulus and area moment of inertia and is calculated by:[11]

$$\overline{EI} = \frac{w}{12} \frac{E_1^2 h_1^4 + E_2^2 h_2^4 + E_1 E_2 h_1 h_2 (4h_1^2 + 6h_1 h_2 + 4h_2^2)}{E_1 h_1 + E_2 h_2} \tag{16}$$

where w is the average width of the unimorph, h_1, h_2 the heights and E_1, E_2 the Young's moduli of the relevant unimorph layer. Figure 4 illustrates the relevant geometry and material parameters for a two layer beam.
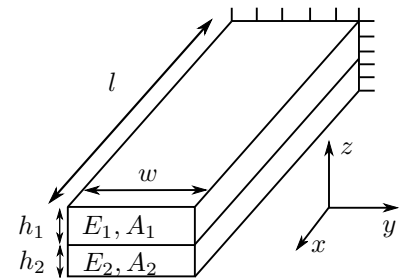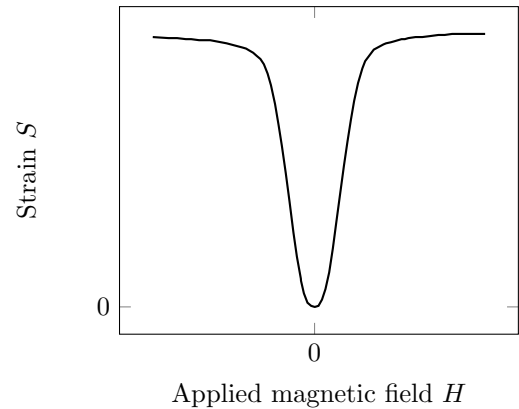

Figure 4: Schematics of a two layer composite with different material parameters

2.2 Magnetostrictive Materials

As early as 1842, the physicist James P. Joule had made observations of length change in iron while applying a magnetic field.[12] From a microscopical point of view an applied magnetic field prompts the magnetic domains inside a material to align with the direction of the external field. The gradual change of the orientation is visible as strain. The greater the field strength, the greater the strain is, up to the point at which every single magnetic moment is orientated towards the field: The material saturates. Figure 5 shows the typical axis-symmetric curve of a magnetostrictive material in the parallel direction. The magnetostrictive behavior is highly nonlinear and therefore it is linearized around a working point. There are different representations for 1D problems all identical one to another. One of them describes the magnetic induction B, also known as magnetic flux density, and the strain S as time and space dependent function of magnetic field H and stress T:[13]

Figure 5: Magnetostrictive behavior

$$\begin{aligned} B(x,t) &= \mu^T \cdot H + d \quad \cdot T(x,t) \\ S(x,t) &= d^* \quad \cdot H + s^H \cdot T(x,t) \end{aligned} \tag{17}$$

where μ^T is the permeability at constant stress, $s^H = 1/E^H$, E^H is Young's modulus at constant field and d, d^* are piezomagnetic and inverse piezomagnetic constants and used in this work synonymously for d_{33}, d_{33}^*. Both are given by $d = (\partial B/\partial T)|_{H=H_0}$ and $d^* = (\partial S/\partial H)|_{T=T_0}$ and can be assumed equal for small perturbations.[13] This representation is appropriate because the material parameters can be easily determined by experimentation.

The preceding paragraph considered the strain and not the stress as input quantity. Therefore, magnetostrictive equations are brought into the form below:

$$B(x,t) = \left(\mu^T - \frac{dd^*}{s^H}\right) \cdot H + \frac{d^*}{s^H} \cdot S(x,t)$$
$$T(x,t) = \qquad -\frac{d^*}{s^H} \quad \cdot H + \frac{1}{s^H} \cdot S(x,t) \tag{18}$$

2.3 Strain

Magnetostrictive materials have an intrinsic relation between strain and magnetic field. Through the coil, changes in magnetic induction inside the material are coupled with the induced voltage. Analyzing the strain contribution along the beam, recommendations about the position of the coil can be deduced. The longitudinal strain $S(x)$ in x-direction can be written as:[14]

$$S(x) = -z\frac{\partial^2 v(x)}{\partial x^2} \tag{19}$$

with $v(x)$ as the deflection curve. The curvature of a fixed-free end long beam is described by the following second order differential equation:

$$\frac{\partial^2 v}{\partial x^2} = -\frac{M_y(x)}{EI} \tag{20}$$

where $M_y(x)$ stands for the bending moment around the y-axis. The bending moment is mainly caused by the relative displacement of the tip mass in reference to the clamping, when being excited. The relative displacement can be described analogously as if a force F is applied at the tip in negative z-axis, causing a bending moment $M_y(x) = F(l-x)$. Hence, the strain is expressed as linear function of the position x:

$$S = z\frac{F(l-x)}{EI} \tag{21}$$

The strain reaches its maximum value at the fixation $x = 0$ and becomes zero at $x = l$.
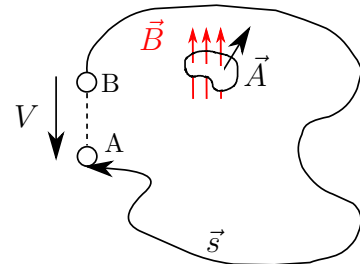
2.4 Electromagnetic Transduction

2.4.1 Electromagnetic Induction

The coil mounted on the magnetostrictive bimetallic stripe transforms the magnetic energy of the deflecting beam into electrical energy through the effect of electromagnetic induction. Faraday's law states that a voltage is induced in a contour surrounding a surface, as long as the magnetic induction of the surrounded area changes. Figure 6 illustrates the conductor loop around a directed area $\vec{A}$ through which a magnetic induction $\vec{B}$ passes. The induced voltage defined as $V = -\oint_{\partial A} \vec{E} \cdot d\vec{s}$ is expressed as:

$$V = \iint_A \frac{\partial \vec{B}}{\partial t} d\vec{A} \tag{22}$$

Figure 6: Conductor loop around a magnetic induction $\vec{B}$ inside an area $\vec{A}$

The magnetic induction mainly changes in the magnetostrictive material since its permeability is much higher than the permeability of air. Furthermore, it is assumed to be constant throughout the cross-section. Considering N contours around the cross section: Every single contour contributes to the induced voltage, depending on the space dependent change in magnetic induction. For sinusoidal signals $\vec{B}_i(t) = \vec{B}_{max,i} \cdot \sin(\omega t)$ the voltage is described as summation of every part:

$$V = \sum_{i=1}^{N} \cdot \vec{A} \cdot \omega \vec{B}_{max,i} \cos(\omega t) \tag{23}$$

With the assumption, that the magnetic field and the cross section are orthogonal, the three-dimensional problem simplifies to an one-dimensional problem. The mean value $\overline{B}_{max}$ of the single parts of the magnetic induction $B_{max,i}$ is introduced with $\overline{B}_{max} = 1/N \cdot \sum_{i=1}^{N} B_{max,i}$. Replacing the time harmonic term $\overline{B}_{max} \cos(\omega t)$ by the root mean square $\overline{B}_{rms}$ leads to Faraday's law:

$$V_{rms} = N \cdot A \cdot \omega \cdot \overline{B}_{rms} \tag{24}$$

In the following sections V and V_{rms} denote the same quantity as well as B and B_{rms}. In case of a constant cross section A which is the case of the considered setup, the magnetic flux $\Phi = B\dot{A}$ is proportional to the magnetic induction B and used synonymously.

2.4.2 Maximum Power Transfer

For wireless applications in addition to the induced voltage the transferred power is a crucial indicator. The deduction bases on a simple electrical series network depicted in Figure 7 with a complex voltage source $\underline{V}$, an equivalent impedance $\underline{Z}_s$ and a load $\underline{Z}_l$. Charles Tevenin has already stated in 1883, that any electrical network with resistances, voltage and current sources can be described as a circuit with an equivalent voltage source and a equivalent series resistance as long as both circuits behaves identically to any load resistance at the terminal AB.[15] The theorem can be generalized to any passive network with inductances and capacitors by means of complex impedances.

The investigated harvester possesses a coil, which operates as a series connection between resistance R_s and inductance L_s. In addition, the magnetic flux change induces a sinusoidal voltage in the coil, represented by the complex voltage $\underline{V}$. Hence, a network results, consisting of the three mentioned parts, while the two latter components are incorporated in the complex source impedance $\underline{Z_s}$. In order to transfer energy, a load impedance is connected to the energy harvester.

Figure 7: Series circuit of a voltage source V, a source impedance $\underline{Z}_s$ and a load impedance $\underline{Z}_l$

Depending on the ratio between source and load impedance a different amount of energy is supplied to the load and will be deduced for the case of a resistive load $Z_l = R_l$ and a complex source impedance $\underline{Z}_s = j\omega L + R_s$. The electrical power transferred to the load is given by the following expression:

$$P(R_l) = V(R_l) \cdot I(R_l) \tag{25}$$

where $V(R_l)$ and $I(R_l)$ are voltage and current of the resistance R_l. Applying Ohm's law for $I(R_l)$ and the complex voltage devider for $V(R_l)/V$ leads to:

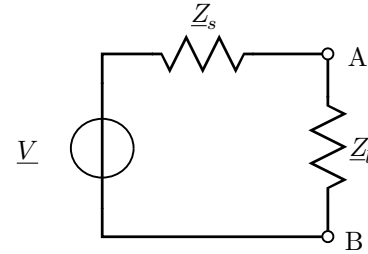$$P(R_l) = V^2 \cdot \frac{R_l}{(R_l + R_s)^2 + (\omega L)^2} \tag{26}$$

The problem can be simplified to the determination of which resistance R_l maximizes the transferred power in relation to R_s and ωL. Solving the extremum problem $\partial P(R_l)/\partial R_l = 0$ delivers the result $R_{l,opt} = \sqrt{R_s^2 + (\omega L)^2}$. If $\omega L \approx 0$, the network can be considered purely resistive and the maximum output power is achieved by matching load with source resistance. There are two cases in which the energy harvester with load resistance can be handled as such a resistive network:

1. Low frequencies
At low frequencies the absolute value of the impedance $Z_{ind} = \omega L$ is much smaller than the resistance R_s. Hence, the resistance dominates and the inductance can be neglected.

2. Complex conjugate matching
In case of high frequencies, the absolute value of the impedance $Z_{ind} = \omega L$ increases and causes higher inductive losses. An appropriate capacitor is added to the circuit and provoke a circulation of the magnetic energy between inductance and capacitor. Complex conjugate matching depicts that theoretically a capacitor C with $C = 1/(\omega^2 L)$ compensates the losses perfectly.

2.4.3 Voltage-Current-Relation and Source Impedance

The inductive losses are minimized due to complex conjugate matching and the network is supposed to be purely resistive. To characterize the dimension, voltage and current are measured at open-circuit V_{open}, short-circuit I_{short} and for different loads. The relation between voltage and current is described by:

$$V = V_{open} - Z_s \cdot I \tag{27}$$

Since the relation is linear, it usually suffices to measure both open-circuit voltage and short-circuit current to draw the slope and obtain the source impedance and hence the optimal load resistance.

2.4.4 Ampere's Law

In the case of a closed circuit in which a load is connected to the circuit, a current flows through the source and load impedance. Whenever a current flows through an inductance a magnetic field is generated and described by Ampere's law.[16] It can be shown that for a long solenoid with N turns, where the length l_c is much larger than the coil radius r_c, the magnetic field of the coil H_c is the superposition of every single wire. It disappears outside the coil and concentrates inside:[17]

$$H_c = \frac{IN}{l_c} \tag{28}$$

Due to Lenz's law the magnetic field is counteracting and decreases the strain which leads to a reduced change in the magnetic induction. A reduced change induces less voltage and therefore a smaller current, which in turn reduces the counteracting magnet field.

2.5 Coil Model

The coil is one main part of the electromagnetic transduction apparatus. Several design parameters can be influenced easily: The coil length l_c, the cross section A_c of the coil, the wire diameter and the number of turns. All parameters mainly influence the electrical source impedance which determines the load and both the output voltage and power. The impedance consists of a series connection of a resistance R_c and an inductance L_c. The resistance R_c is mainly a function of the coil contour and number of turns but depends also on the coil length, because the length influences the number of layers. For the same amount of turns, a shorter coil has more layers than a longer coil. With every layer the contour of the wire increases and so the resistance increases as well. Noteworthy is that the resistance increases with a high amount of windings quadratically, which is shown below. The coil is assumed to be shaped rectangularly such as the unimorph and has a width w_c and height h_c. A wire with N turns surrounds the coil. It is characterized by the resistivity ρ_{el}, the total wire diameter d_t which is composed of the wire diameter d_w and an offset. The offset takes into consideration the space between the turns, created during the winding process. Since the isolation layer is very thin compared to the conductive core, it is neglected. To determine the resistance it is sufficient to calculate the total wire length l_t. Every layer has a different contour and holds at most $k = l_c/d_t$ turns. For a given geometry and wire diameter, the number of layers k then depends on the number of turns and is determined by $n = N/k$ for fully occupied layers. The contour of the first layer equals $l_{l,1} = 2(w_c + h_c)$. Every further layer increases the effective contour. Both width and height are extended by twice the wire diameter. For round wires, every layer is slightly displaced as shown in Figure 8. For small offsets compared to the wire diameter, the displacement is scaled by the factor $\sqrt{3}/2$.

$$l_{l,2} = 2 \cdot \left(w_c + h_c + 4 \cdot \frac{\sqrt{3}}{2} d_w\right) \tag{29}$$

$$l_{l,2} = 2 \cdot (w_c + h_c + 2\sqrt{3} d_w) \tag{30}$$

$$l_{l,3} = 2 \cdot (w_c + h_c + 2 \cdot 2\sqrt{3} d_w) \tag{31}$$

$$l_{l,n} = 2 \cdot (w_c + h_c + (n-1) \cdot 2\sqrt{3} d_w) \tag{32}$$

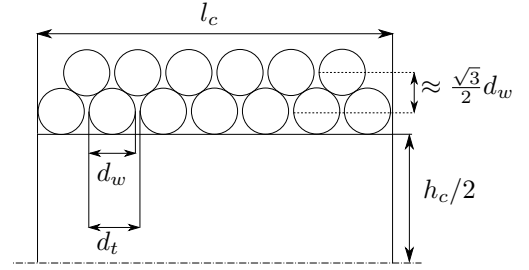In order to get the total length, all wires have to be summed:

$$l_t = k \cdot \sum_{i=1}^{n} l_{l,i} \quad (33)$$

$$l_t = 2(w_c + h_c)k \cdot n + 4\sqrt{3}d_w k \cdot \sum_{i=1}^{n}(i-1) \quad (34)$$

$$l_t = 2(w_c + h_c)k \cdot n + 4\sqrt{3}d_w k \cdot \frac{(n-1)^2 + (n-1)}{2} \quad (35)$$

$$l_t = 2(w_c + h_c)k \cdot n + 2\sqrt{3}d_w k \cdot (n^2 - n) \quad (36)$$

$$l_t = 2\sqrt{3}d_w d_t/l_c \cdot N^2 + 2[(w_c + h_c) - \sqrt{3}d_w] \cdot N \quad (37)$$

Figure 8: Cross section of a pick up coil with two wire layers

If the wire diameter d_w is much smaller than the sum of $w_c + h_c$, Equation 37 can be simplified to:

$$l_t = 2\sqrt{3}d_w d_t/l_c \cdot N^2 + 2(w_c + h_c) \cdot N \quad (38)$$

Equation 38 shows a quadratic dependency. With the knowledge of the wire length, the electrical resistance can be calculated by:

$$R_c = \rho_{el}\frac{l_t}{A_{wire}} = \rho_{el}\frac{4l_t}{\pi d_w^2} \quad (39)$$

For later applications, the resistance is reformulated as function of N into

$$R_c = r_{s2} \cdot N^2 + r_{s1} \cdot N \quad (40)$$

where $r_{s2} = 8\sqrt{3}d_t\rho_{el}/(l_c\pi d_w)$ and $r_{s1} = 8(w_c + h_c)\rho_{el}/(\pi d_w^2)$. For general statements, the inductive behavior estimate is significantly reduced with the model for a long cylindrical coil. The inside of the coil contains the magnetostrictive material, air and the non-magnetic support material of the coil. Since magnetostrictive materials conduct the magnetic induction many times better than air, only the cross section of the magnetostrictive material is considered in order to calculate the inductance:

$$L_c = \frac{\mu_0\mu_r w_{ms}h_{ms}}{l_c}N^2 \quad (41)$$

where w_{ms} and h_{ms} are the width and height of the magnetostrictive cross section A_{ms}, μ_0 the vacuum permeability and μ_r the relative permeability of the magnetostrictive material. Equation 41 can only roughly illustrate a general trend. This is especially because the permeability as a magnetic property depends both on the applied stress and on the biased magnetic field applied through the permanent magnets. The impedance of the coil results in

$$Z_c = \sqrt{R_c^2 + (\omega L_c)^2} \quad (42)$$

The wire length not only influences electrical but also mechanical properties, in particular the total mass, in case the coil is fixated on the beam. The mass of the pick-up coil m_c can be expressed as

$$m_c = m_{sup} + m_w \quad (43)$$

$$m_c = m_{sup} + \rho_{mech}\frac{\pi d_w^2}{4} \cdot l_t \quad (44)$$

where m_{sup} is the mass of the support of the pick-up coil, m_w the mass of the wire and ρ_{mech} the density of the core material of the wire, which is typically copper.

3. PARAMETER STUDIES

Various coil designs change the properties and impact the energy transformation: The coil geometry determines length, height and width, thus the electrical impedance as well as the covered magnetostrictive area. The number of turns characterizes output voltage and coil impedance as well. Unequal magnetic flux change along the beam leads to examining the position of the pickup coil.

3.1 Coil Positioning

As stated in Section 2.3, the strain S of the unimorph energy harvester linearly decreases along the position z. The magnetic domains of the magnetostrictive material change the orientation when they are strained, leading to a coupling of magnetic induction and strain. Figure 9 schematically illustrates the orientation of the magnetic domains along a deflected beam. For small deflections, both quantities are considered directly proportional as described by the piezomagnetic Equations 18.

When the beam resonates, the amplitude of the magnetic induction oscillates between $-B_{max}(x)$ and $B_{max}(x)$ and determines the induced voltage. Linear modelling indicates that the greater the distance of the coil, the smaller the generated voltage. Further, it is supposed to neglect the friction between coil and beam.
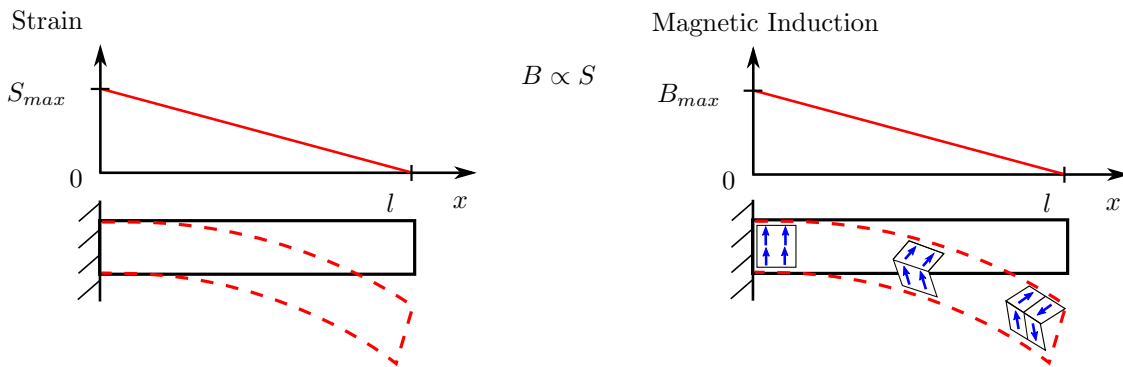
Figure 9: Correlation between strain S and magnetic induction B for a deflected magnetostrictive beam

3.2 Coil Contour

According to Faraday's law the induced voltage is derived as circulation of the electric field $\vec{E}$ along the path ∂s and depends only on the change in magnetic induction $\partial \vec{B}/\partial t$ in the area $\vec{A}$ encircled by the contour. If the change in magnetic induction is constant within the cross section A, the circulation of the electrical field is path-independent. As mentioned, the magnetostrictive material has a much higher permeability than the non-magnetic support layer and air. Thus it is supposed that the entire magnetic induction is driven through the constant cross section of the magnetostrictive material. Hence, the induced voltage can be considered path-independent. Figure 10 briefly illustrates the circulation of the magnetic induction.
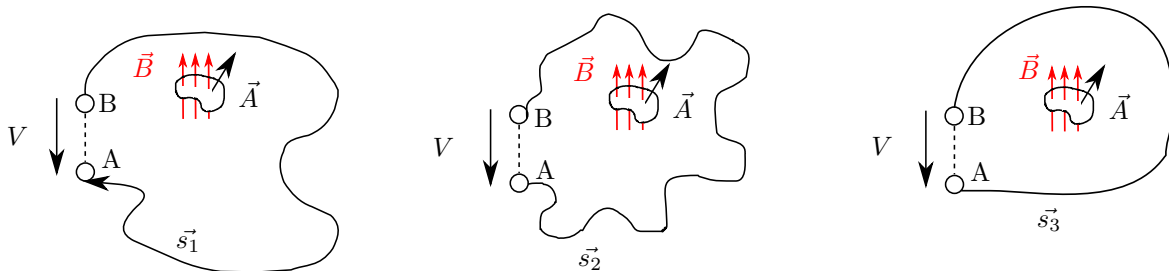
Figure 10: Different wire contours encircle the same oriented area $\vec{A}$ with the time-dependent magnetic induction $\partial \vec{B}/\partial t$ and the same voltage V is generated in all three cases

At the terminal AB of all three wire contours, the measurable voltage is identical for time harmonic changes of the magnetic induction. A distinct difference appears when the power is analyzed which is indirectly proportional

to the resistance. A small contour requires a short wire and has a small resistance, which is the case of a tightly mounted coil. Aside this coil adds stiffness, mass and unfavorably changes the damping of the system. A wider wound coil has a longer wire and a greater resistance, but does not impact the mechanical properties. Experiments will indicate if the advantages of a smaller resistance of a tightly mounted coil outbalance the mechanical issues in comparison to wider wound coils.

3.3 Number of Turns of the Coil

The analysis of Faraday's law reveals a linear correlation between the number of turns and the output voltage. As derived in Section 2.5 the number of turns impacts the source impedance and hence the output power. In addition the current creates a magnetic field inside the coil and a negative feedback occurs. In literature, different approaches have been regarded.

In 2008, Wang and Yian derived the global electromechanical coupling factor from the internal energy $\varepsilon = 1/2 \cdot S \cdot T + 1/2 \cdot H \cdot B$, the linearized constitutive magnetostrictive equations and assuming an ideal solenoid coil. Since the obtained coupling factor is independent on the number of turns, the authors made similar statements for the output power.[2] Deng and Dapino assumed that the magnetomechanic damping of the beam caused by an interaction with the magnetic field of the coil is negligible in regard to the mechanical damping. They validated the assumption according to their specific setup.[18] From their models, a linear correlation between power and number of turns for low frequencies can be concluded. Another approach is derived, using the linearized magnetostrictive equations and assuming:

- A constant magnetic field inside the coil $\leftrightarrow$ Long solenoid
- No mechanical influence of the coil
- Negligible feedback from the magnetic domain into the mechanical domain

The expression of the negative magnetic field of the coil $-H_c$ due to Lenz law replaces the magnetic field H in the linearized constitutive magnetostrictive equation 18:

$$\overline{B} = \left(\mu^T - \frac{dd^*}{s^H} \right) \cdot H + \frac{d^*}{s^H} \cdot \overline{S} \tag{45}$$

The magnetic field of the coil H_c results from Ampere's law given by Equation 28: $H_c = N \cdot I / l_c$. The current of the coil is determined by Ohm's law $I = V/Z$. Assuming conjugate complex matching, the inductance is negligible. The impedance is the sum of coil and load resistance $Z = R_l + R_c$. Further, the load resistance R_l is specified as multiple of R_c such that $R_l = k \cdot R_c$. The voltage is specified by Equation 24: $V = N \cdot A \cdot \omega \cdot \overline{B}$. Inserting the equations above in Ampere's Law leads to an expression of the magnetic field inside the coil:

$$H_c = \frac{N^2 \cdot A \cdot \omega \cdot \overline{B}}{l_c \cdot (k+1) \cdot R_c} \tag{46}$$

The magnetic field is replaced in Equation 45 and the equation is rewritten:

$$\overline{B} = \frac{d^* / s^H}{1 + \left(\mu^T - \frac{dd^*}{s^H} \right) \cdot \frac{N^2 \cdot A \cdot \omega}{l_c \cdot (k+1) \cdot R_c}} \cdot \overline{S} \tag{47}$$

Equation 47 represents the magnetic induction as an independent function of the magnetic field H. To simplifiy analysis, the total induced voltage is written as function of N and R_c and determined by:

$$V_{tot} = \frac{c_1 \cdot N \cdot (k+1) \cdot R_c}{(k+1) \cdot R_c + c_2 \cdot N^2} \tag{48}$$

with the constants $c_1 = A \cdot \omega \cdot d^* / s^H \cdot \overline{S}$ and $c_2 = (\mu^T - dd^*/s^H) \cdot A \cdot \omega / l_c$. Material parameters and the windings influence the feedback and the induced voltage. Further, the load resistance regulates the current and hence the negative feedback. Expressions for the effective source resistance and the transferred power are deduced. Based on the voltage-current-relation and rewriting Equation 27, the source resistance can be expressed as:

$$R_s = \frac{V_{open} - V}{I} \tag{49}$$

In the open-circuit, no current flows. This holds true if the load resistance is infinite and is described in Equation 48 for $k \to \infty$. Consequently, the open-circuit voltage may be computed by

$$V_{open} = c_1 \cdot N \tag{50}$$

which is identical to the proportional relation between number of turns and induced voltage of Faraday's law. The voltage V is defined as voltage between the terminal AB and equals the voltage drop over the load resistance. It is calculated by the voltage divider $V = R_l/(R_l + R_s) \cdot V_{tot}$ in which R_l/R_c is replaced by k:

$$V = \frac{c_1 \cdot N \cdot k \cdot R_c}{(k+1) \cdot R_c + c_2 \cdot N^2} \tag{51}$$

Inserting Equation 50, 51 and Ohm's law $I = V/R_l$ in 49 ends up in:

$$\boxed{R_s = R_c + c_2 \cdot N^2} \tag{52}$$

Equation 52 clearly indicates, that the source resistance is the sum of the coil resistance R_c, and the term $c_2 \cdot N^2$, which is related to material, geometry and windings. The maximum output power is obtained at $R_l = R_s$, such that the load resistance has to be greater than the simple coil resistance R_c. The load resistance controls the current which impacts the magnetic feedback. On the one hand, a higher load resistance limits the total current. On the other hand, smaller currents result in less feedback. Thus, the optimal load resistance is shifted away from R_c. With the knowledge of the source impedance, the maximum power for the load can be calculated. For $R_l = R_s$ follows $k = 1 + c_2 \cdot N^2/R_c$ and the maximal output over the resistance R_l is expressed by:

$$P_{max}(R_l = R_s) = \frac{(c_1 \cdot N)^2}{4 \cdot (R_c + c_2 \cdot N^2)} \tag{53}$$

According to Equation 40, the coil resistance R_c can be expressed as function of number of turns $R_c = r_{s2} \cdot N^2 + r_{s1} \cdot N$. Replacing R_c in 53 and after simplifying, the maximum transferred power is described as:

$$\boxed{P_{max} = \frac{c_1^2 \cdot N}{4 \cdot \big[(c_2 + r_{s2}) \cdot N + r_{s1}\big]}} \tag{54}$$

Both numerator and denominator in Equation 54 are of degree one. In the case of huge number of turns and the assumption of a long solenoid can still be fulfilled, the output power remains constant and does not increase with the windings N. For moderate numbers ($N << r_{s1}/(c_2 + r_{s2})$) the output power increases linearly.

3.4 Coil Length

The coil length is closely related to both, the positioning of the coil and the counteracting magnetic field of the coil. Considering two coils with the same number of turns, but different coil lengths as Figure 11 schematically illustrates, the shorter coil covers an area of higher average magnetic flux than the longer coil. Ideally, an optimally placed short coil will have a high induced voltage. At the same time a shorter coil requires more wire layers and thus the resistance tends to rise more quadratically than linearly, which in turn impacts the output power. Further, a longer coil reduces the counteracting magnetic field. The result is a coil length as compromise between coil resistance, negative magnetic field and average change of magnetic induction.

For general statements about the coil length, Equation 54 is restructured as function of the coil length l_c. The coil length impacts the constants r_{s2} and c_2. From both constants, the constants $r'_{s2} = r_{s2} \cdot l_c$ and $c'_2 = c_2 \cdot l_c$ are

(a) Short coil   **(b)** Long coil

Figure 11: Example of two different long coils, placed at the fixation of the beam

derived which are independent of the coil length l_c. In addition, the constant c_1 contains the average deflection $\overline{S}$, covered by the coil, defined as:

$$\overline{S} = \frac{\mathbf{S}(x_1 + l_c) - \mathbf{S}(x_1)}{l_c} \qquad \text{with} \quad x_1 + l_c \leq l \qquad (55)$$

where $\mathbf{S}(x)$ is the primitive of the strain distribution $S(x)$ along the beam. The average deflection appears to be a function of coil length. Therefore the constant c'_1 is defined as $c'_1 = c_1 / \overline{S}$. With this knowledge the open-circuit voltage and maximum output power as function of the coil length l_c are given by:

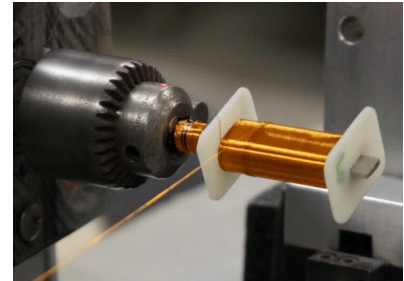$$V_{open}(l_c) = \frac{c'_1 \cdot \Big(\mathbf{S}(x_1 + l_c) - \mathbf{S}(x_1) \Big) \cdot N}{l_c} \qquad (56)$$

$$P_{max}(l_c) = \frac{\Big[c'_1 \cdot \Big(\mathbf{S}(x_1 + l_c) - \mathbf{S}(x_1) \Big) \Big]^2 \cdot N}{4 \cdot \Big[(c'_2 + r'_{s2}) \cdot N \cdot l_c + r_{s1} \cdot l_c^2 \Big]} \qquad (57)$$

Equation 57 describes the power as function of length. It depends on strain contribution, material and geometry parameters. Normalization to $c'^2_1 / N \cdot 4$ simplifies further analysis. Plotting the normalized power as function of length for appropriate values will indicate the optimum coil length. It can also be calculated by solving the extremum problem $\partial P_{max}(l_c) / \partial l_c = 0$.

4. EXPERIMENTAL SETUP

4.1 Coil Manufacturing

The investigation of different coil parameters necessitates different coils which are all manufactured in a homogeneous winding process. The first step starts with the design of a support, on which the wire is wound. The support was processed by a 3D-printer. A semi-automated coil winder was used for the second fabrication step in which the wire was wound around the pickup coil. As depicted in Figure 12, the coil winder consists of a controllable drilling head, a metal piece with one cylindrical side, spanned into the drilling head and with one cuboid side, containing the mounted coil support. By means of a threaded spindle the wire was precisely guided and a laser displacement sensor was used to count every single rotation of the drilling head. Thus, the coil support rotated homogeneously and improved the winding process. As a compromise between rapidity and accuracy, gaps appear due to the small

Figure 12: Drilling head and coil during the winding process

wire diameter and propagate in every further layer. Since gaps are considered as unused space and less turns per layer, they need to be eliminated regularly when high number of turns are desired. Consequently, after ten layers, a thin layer of tape was adhered on a completed layer to create a flat and homogeneous surface. Three different types of coils were manufactured and tested. Coils with:

- Constant number of turns N and varied lengths l_c
- Constant length l_c and varied number of turns N
- Constant number of turns N and different contours

While length and number of turns can be chosen arbitrarily, the geometry of the unimorph and the minimum layer thickness of the 3D printer of 1 mm dictate the minimal inner and outer contour of the coil.

Two series of well-fitted coils, using wires with a diameter of $d_w = 0.127$ mm (wire gauge #36), were produced to validate the developed coil model from Section 2.5. Due to the dimension of the unimorph beam of 6.4 mm x 1.9 mm, the printed coil supports had an outer contour of $w_c = 8.5$ mm and $h_c = 4.1$ mm. The inductance was measured for the coils placed at the fixation on a 3 inch long titanium-galfenol sample. Galfenol was bonded on a titanium support for high temperature applications. The exact dimensions of the titanium-galfenol sample are given by w_{Ga}=6.32 mm, h_{Ga}=0.67 mm, w_{Ti}=6.40 mm, h_{Ti}=1.17 mm and l=77,8 mm. The effective length, indicating the distance between the clamping and the tip mass, is 64 mm. Figures 13 illustrates calculated and measured values for resistance, inductance and wire mass, supposing a resistivity of $\rho = 1.69 \cdot 10^{-2} \, \Omega \cdot mm^2/m$, a density of $\rho_{mech} = 8.96$ g/cm^3 and an average distance of $d_t = 0.158$ mm between each wire. The average distance is larger than the wire diameter due to an additional thin isolation layer, minimal space between every wire and imperfect winding.
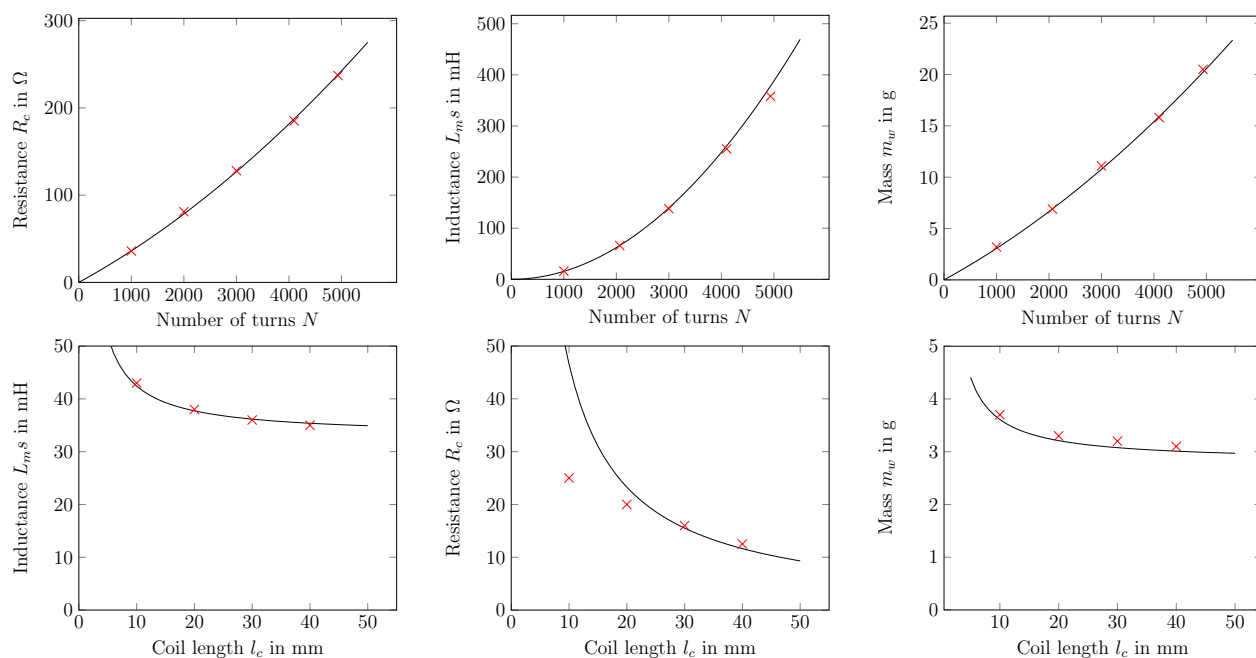

Figure 13: Modeled and measured values (red points) for resistance, inductance and mass for two manufactured coil series

Since exact measurements for the relative permeability of small samples are difficult, a relative permeability μ_r of 87.5 was assumed and resulted from the mean value of the declared range (for galfenol between $75 < \mu_r < 100$) of the material producer ETREMA. As illustrated in Figure 13, the measured quantities coil resistance and mass fit very well with the predicted values for different number of turns and for different coil lengths. The inductance deviates for small lengths significantly. In particular the 10 mm and 20 mm long coil does not fulfill the requirements of a long cylindrical coil, whose length is much greater than the coil diameter. Furthermore, the inductance also depends on the applied stress on the unimorph, the biased magnetic field and the position along the unimorph. This makes the determination of the relevant relative permeability difficult. Additional coil series were fabricated for the above mentioned investigations, their geometry and properties are listed at the relevant sections.

4.2 Setup for Analyzing the System Performance

A common method to characterize vibrational energy harvesters is based on measuring the frequency response of the open-circuit voltage and the transferred power. To obtain the frequency response, a permanent magnet shaker (model: Labwork ET-139) was used and created harmonic excitations over a desired frequency rang. Due to the permanent magnetic field of $2\,\mathrm{kA/m}$ on the bottom of the shaker, a steel plate was joined with four $15\,\mathrm{cm}$ long brass rods and mounted on the shaker. At that distance, the field only had a negligible value of $0.16\,\mathrm{kA/m}$. In order to reduce disturbances created by the rods, several layers of copper wire were wrapped around to stabilize the structure. The measured acceleration signal, obtained with a pieozoelectric accelerometer (model: PCB Piezotrinics 333B50), was equal for the bottom and top of the construction. Figure 14 shows the complete setup with the magnetostrictive unimorph energy harvester, an accelerometer, on top of the shaker and steel stand-off plate.

Measuring the frequency response faces the problem, that the resonating system is very sensible at resonance frequency and controlling the base excitation is challinging. Furthermomre in pratice a resonating system vibrates with a given frequency and amplitude. When a harvester is mounted on the system and absorbs energy, the total base excitation decreases. There was no controller which adapted the input signal so that the amplitude of the base excitations kept constant within a variation of 1%. That is why beforehand the input signal of the shaker was kept constant over the desired frequency range without mounted energy harvester. Instead a dummy mass was mounted, having the same mass of the energy harvesting system. The output signal, provided by the accelerometer, was evaluated and used to adapt the input signal of the shaker. Once the base excitations without energy harvester were precise enough, the energy transducer could be mounted and parameters were studied.
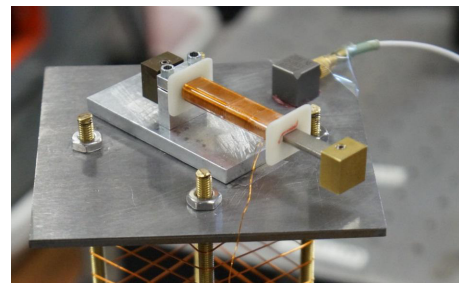

Figure 14: Setup for harmonic base excitations: Energy Harvester with accelerometer, steel stand-off plate and shaker

5. EXPERIMENTAL RESULTS

The power is calculated using the open-circuit voltage and the short-circuit current. This is valid in case of a linear relationship. For resistive networks with negligible inductance it is experimentally shown, that the energy harvester can be treated as a voltage source and a source resistance, regarding the system from the electrical terminal. In that case the resistance includes not only the coil resistance but also all magnetic and mechanical effects, which are also transferred into the electrical domain.[19] For experimental proof of the voltage-current relation, the 3 inch long titanium-galfenol sample was used with an effective length of $64\,\mathrm{mm}$. NdFeB magnets of type B442-N52, provided by K&J Magnetics Inc., created a biasing field.[20] A coil with 1120 turns was mounted on the beam at the point of fixation without touching the harvester. Figure 16 shows the voltage-current-and resistance-power relation for a base excitation of $\hat{a} = 0.1\,\mathrm{g}$. While current, voltage and deflection are described as root-mean-square values, the base excitation is expressed as peak value. The relations were obtained by connecting different resistive loads to the pickup coil as illustrated in Figure 15, by measuring the voltage drop over the load resistance and calculating the current backwards.
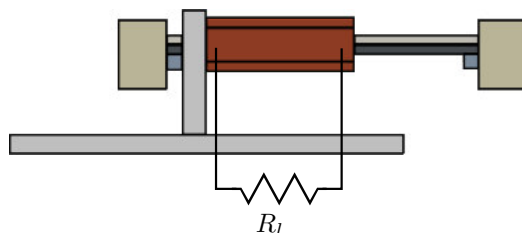
Figure 15: Schematic of the magnetostrictive unimorph energy harvester with connected load resistance R_l

(a) Voltage-current-relation

(b) Power-resistance-relation
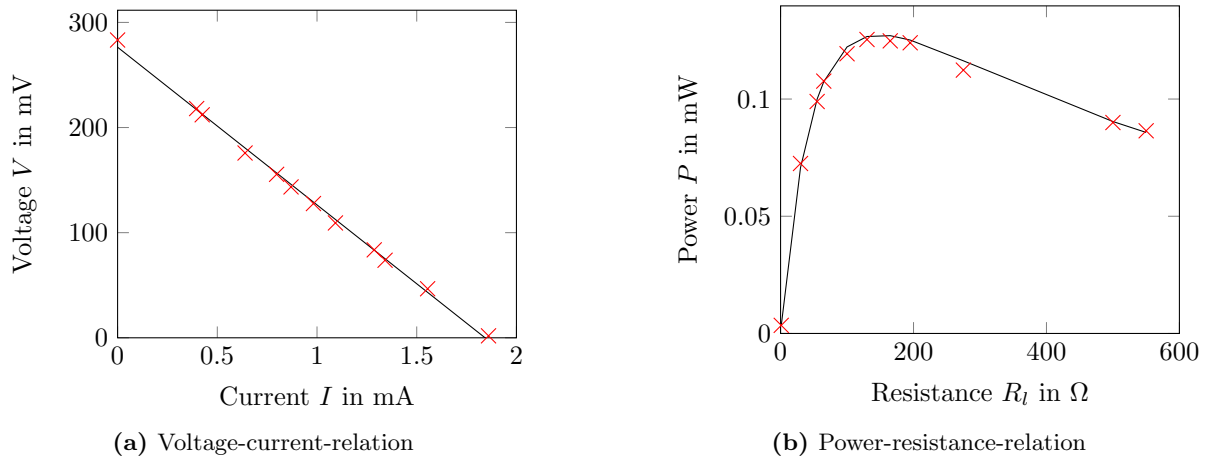
Figure 16: Electrical port properties - measured (red points) and ideal values (black line) for a titanium-galfenol unimorph with a 30 mm long non-touching coil with $N = 1120$ and a base excitation of $\hat{a} = 0.1\,\mathrm{g}$ at $f_0 = 93.6\,\mathrm{Hz}$

As demonstrated previously, the harvester can be simplified as an electrical circuit with a voltage source and a source resistance. Since other configurations behaved in a similar way, it suffices to measure the quantities open-circuit voltage and short-circuit current. If the inductance becomes relevant, both quantities are nevertheless enough to determine the source impedance and hence the optimal load resistance by applying Ohm's law. This method enormously simplifies the amount of measurements and is applied to the following parameter studies.

In order to detect irregularities during the measurements, at least three resistances were used in addition to the open-circuit and short-current case. As a narrow band energy harvester, the magnetostrictive unimorph harvester has a very small range of high performance. Therefore, first a coarse frequency sweep indicated the resonance frequency. Afterwards, a second sweep with a step of $\Delta f = 0.2\,\mathrm{Hz}$ close to the resonance frequency presented more accurate results.

5.1 Coil Contour

Two coils were manufactured in order to compare the influence of a closely wound coil and a non-touching coil. Their properties are listed in Table 1. A non-touching pickup coil has to incorporate an equal distance to the unimorph beam from the top and bottom edge. Its borders are widened, such that they lay on the ground and enable a fixation with the ground. Then the coil was connected with double sided tape to the metal and the borders were enlarged, so that the coil core could be connected with the ground, too. Figure 17 shows the measurements from Coil 1 and Coil 2 with respect to voltage and power for different distances to the beam fixation.

Coil	Inner dimension in mm x mm	Outer dimension w_c x h_c in mm x mm	m_{sup} in g	m_c in g	R_c in Ω
1	2.2 x 6.6	4.2 x 8.8	1.7	5.4	43
2	5.0 x 8.4	7.0 x 10.6	2.6	7.4	56

Table 1: Properties for coils with different contours, length $l_c = 30$ mm and number of turns $N = 1120$.

Both diagrams demonstrate the loss of performance for the closely connected Coil 1. Induced voltage and maximum transferred power are significantly higher, using Coil 2, in spite of a higher coil resistance. Remarkably, that Coil 1 is not performing the best at the fixation but between a distance of 10 mm and 15 mm. Measuring the deflection at the tip and the resonance frequency provides an explanation. The resonance frequency decreases with the distance of Coil 1 to the fixation, since the mass of the coil has a stronger impact with rising distances.
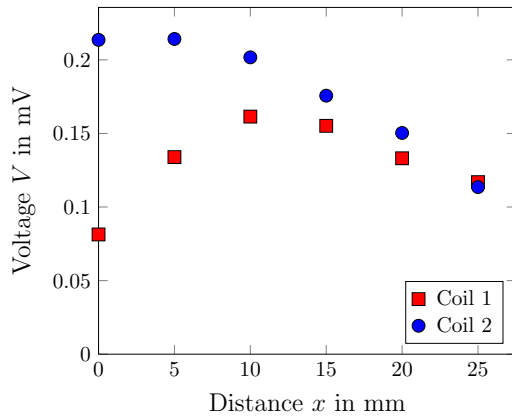
(a) Open-circuit voltage for Coil 1 and 2
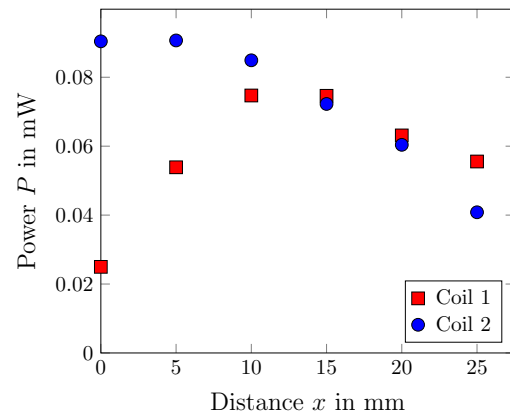
(b) Transferred power for Coil 1 and 2

Figure 17: Open-circuit voltage and output power of a non-touching and a touching coil as function of the distance x to the fixation

Furthermore, the resonance frequency measured close to the fixation is higher than the constant resonance frequency of Coil 2. This underlines that Coil 1 increases the stiffness of the system. Besides the worse performance of a closely wound coil due to mechanical effects, it is challenging to predict the stiffness created by a closely wound coil and hence the resonance frequency. For this reason, the following parameter studies are reduced to non-touching coils.
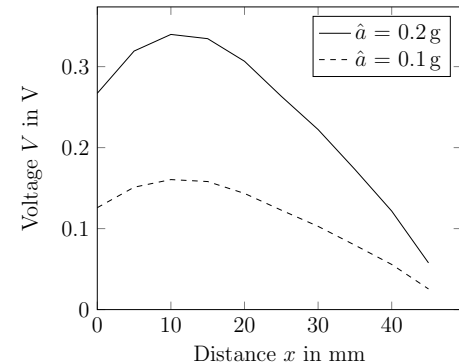
5.2 Coil Positioning

The investigation of the coil contour have already shown trends where a higher induced voltage and hence output power can be harvested. The recent setup was modified such that a 10 mm long Coil with N=750 provided four more values than the 30 mm long coil. It also guaranteed a higher resolution since the turns cover a smaller area of magnetostrictive material in which the strain is averaged over a smaller length. The open-circuit voltage is considered as indicator for the following experiments, whose results are depicted in Figure 18.

Figure 18: Induced voltage as function of the distance for a 10 mm long coil

The plot shows a decreasing parabolic part from 0 mm to 20 mm with a maximum at about 10 mm and a linearly falling part from 20 mm to 45 mm. While the second part agrees with the assumption that the change of magnetic flux decreases linearly with the distance as the strain does, the first part differs. It depicts that the highest voltage is not obtained at the fixation.

Since Yoo and Flatau[21] confirmed a correlation between biasing magnetic field and Young's modulus, different biasing magnets were used. Using different magnets did not affect the trend and affected the resonance frequency only marginally.

The following studies of the coil length in the next section bases on the concrete strain distribution along the beam. Due to the linear relation between strain, magnetic induction and voltage in the open-circuit case, the measurement curve from Figure 18 with $\hat{a} = 0.2\,\text{g}$ is described as normalized strain contribution. Further the x-axis which denotes the distance has to be shifted. The coil placed at 10 mm can be treated as a lumped element at 5 mm + 1 mm. The added value takes into account the 1 mm thick coil frame. In that case the normalized strain contribution is described as:

$$\frac{S(x/l)}{S_{max}} = 4.08 \cdot x^3 - 8.37 \cdot x^2 + 3.67 \cdot x + 0.54 \tag{58}$$

5.3 Coil Length

Three more coils with the same number of turns were manufactured with the lengths 20 mm, 30 mm and 40 mm. To obtain comparable results, all coils are supposed to have a completed wire layer. Therefore, the lowest common multiple of turns resulted in about 750 turns. The properties of each coil are listed in Table 2. It is assumed that the coil begins at the clamp, since in practice it is easier and more reliable than a fixation in the middle of the beam. Knowing the induced voltage as function of the position allows the prediction of values for different lengths. According to Section 3.4, the anticipation of the induced voltage acts on the assumption of magnetic feedback and an averaged strain contribution along the coil length.

Coil	l_c in mm	Layer	m_w in g	R_c in Ω	L_{ms} in mH*
3	10	12	3.3	38.3	12
4	20	6	3.0	35.1	10
5	30	4	2.9	34.4	9
6	40	3	2.9	34.1	6

Table 2: Properties of coils with different lengths, a rectangular outer contour of 9.5 mm x 6.5 mm and $N = 750$

Based on Equations 56, 57 and 58, normalized open-circuit voltage and optimal power are calculated and compared with normalized measurements of the four different long coils. The coil length l_c was normalized to the beam length $l = 64$ mm and the voltage and power to the maximum values. Both are illustrated in Figure 19.
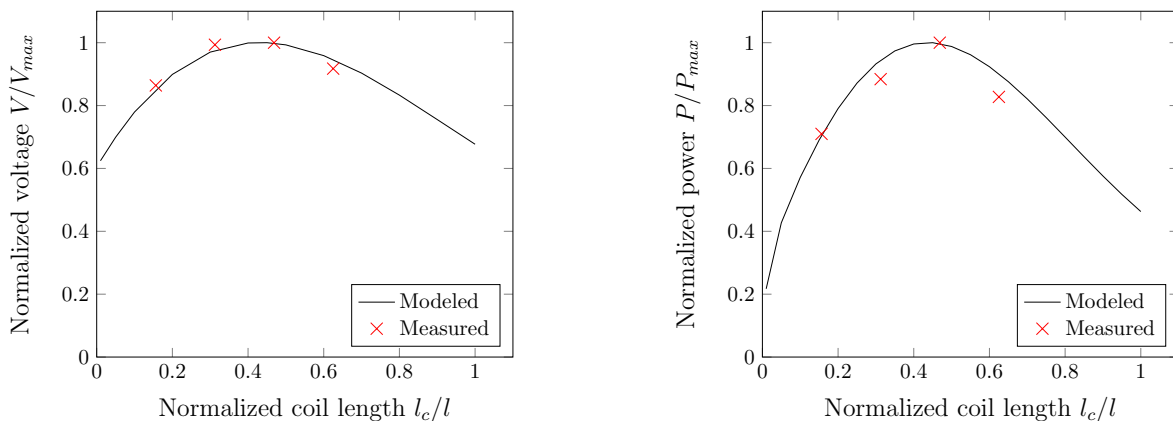
Figure 19: Normalized open-circuit voltage V/V_{max} as function of normalized coil length l_c/l for modeled and measured values

Modeled and measured values match very well. The best results are obtained for a coil with the length $l/l_c \approx 0.45$, relating to the length of 28.8 mm. This explains the best performance of the 30 mm long coil.
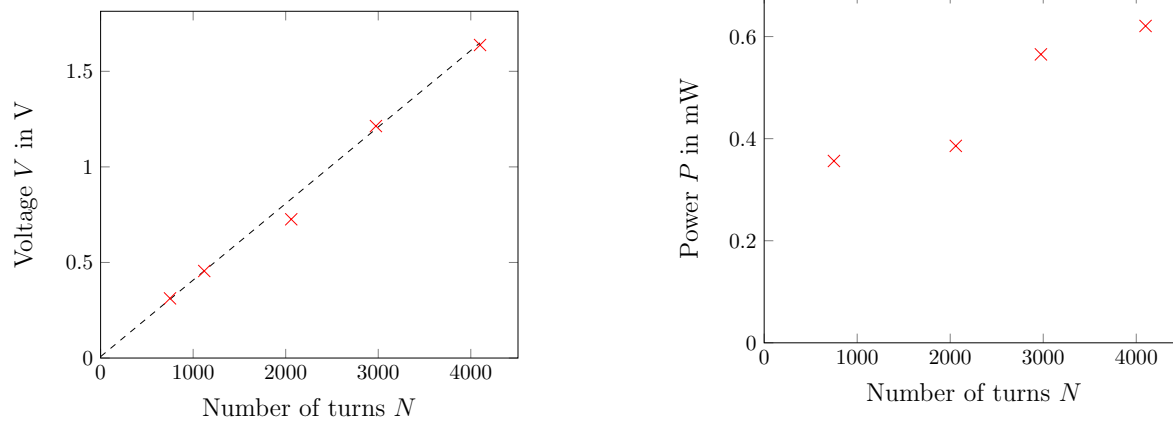
5.4 Number of Turns

In the previous section, best results could be obtained with the 30 mm long non-touching coil, placed at the fixation of the 64 mm long titanium-galfenol beam. In order to study the number of turns N, three more 30 mm long coils with the same cross section and an outer dimension of w_c x $h_c = 9.5$ mm x 6.5 mm were manufactured to provide enough measurements. Additionally, another 30 mm coil with 1120 turns was taken to provide one more value for the open-circuit voltage. Due to its different cross section, it was not used for output power measurements. Table 3 presents an overview of the properties of the fabricated coils.

Figure 20 illustrates the correlation between a higher number of turns, the induced voltage and the maximum output power at optimum load $R_{l,opt}$ at resonance frequency $f_0 = 94$ Hz.

Coil	Turns N	Layer	m_{coil} in g	R in Ω	L_{ms} in mH
5	750	4	2.9	34	12
7	2060	11	11.5	101	66
8	2975	16	15.9	153	138
9	4100	22	22.3	228	251

Table 3: Properties for coils with different lengths, w_c x h_c = 9.5 mm x 6.5 mm and $N = 750$ turns

Figure 20: Open circuit voltage V and transferred power P as function of number of turns N for a base excitation of $\hat{a} = 0.2\,\text{g}$

As predicted, the induced voltage V increases linearly with the number of turns N. The data point $N = 2060$ differs from the regression and was due to a loose fixation, that affected beam and coil integrity, thus suppressing the deflection. The measurements also indicate an increase of the transferred power at optimum load and refutes the assumption from Wang and Yang that the number of turns does not impact the achievable power.[2] The slope is not linear but continuous and a result of both the quadratically increasing inductive impedance ωL_{ms} and magnetic feedback. A matching capacitor would improve the performance and lead to a higher output power. At this point, appropriate capacitors were not available.

6. CONCLUSION

In this study, the theoretical fundamentals of describing a magnetostrictive unimorph energy harvesters have been stated and existing models have been extended. A special focus was given to the design of a pickup coil as an eletromagnetic transducer. A model, characterizing the coil impedance was established and experimentally verified. A closely wound coil influences the material parameters and finally makes the determination of the resonance frequency challenging. Thus, the established concept of recent work using a closely wound coil was questioned and the coil contour investigated: A comparison of a non-touching coil with a larger impedance outperformed a closely wound coil. Models and experiments proved, that the output voltage and power can be increased by means of a higher number of turns. During experimentation a decrease of the output power due to more turns could not be observed. Studying the voltage as function of coil position represented the strain contribution. Contrary to the exception, it did not decrease linearly. Based on the specific contribution, the optimal coil length was theoretically determined and confirmed by measurements. Due to the non-linearly decreasing strain along the beam, first it is recommended to estimate the strain profil. Then the specific coil length and position can be determined in order to maximize the energy transformation process.

Besides the investigated coil parameters the wire diameter remained. Future work could deal with the wire diameter in order to show the compromise between a higher resistance due to a smaller wire cross section and higher induced voltage as result of more windings per space. The presented statements are not restricted to magnetostrictive unimorph harvester, since all magnetostrictive harvesters have to deal with electromagnetic induction.

REFERENCES

[1] Kim, H. S., Kim, J.-H., and Kim, J., "A review of piezoelectric energy harvesting based on vibration," *International Journal of Precision Engineering and Manufacturing* **12**, 1129–1141 (dec 2011).

[2] Wang, L. and Yuan, F. G., "Vibration energy harvesting by magnetostrictive material," *Smart Mater. Struct.* **17**, 045009 (jun 2008).

[3] "Composite magnetoelectrics," (2015).

[4] Yoo, J.-H. and Flatau, A. B., "A bending-mode galfenol electric power harvester," *Journal of Intelligent Material Systems and Structures* **23**, 647–654 (feb 2012).

[5] Ueno, T. and Yamada, S., "Performance of energy harvester using iron-gallium alloy in free vibration," *IEEE Trans. Magn.* **47**, 2407–2409 (oct 2011).

[6] Kita, S., Ueno, T., and Yamada, S., "Improvement of force factor of magnetostrictive vibration power generator for high efficiency," *J. Appl. Phys.* **117**, 17B508 (may 2015).

[7] Ueno, T., "Performance of improved magnetostrictive vibrational power generator, simple and high power output for practical applications," *J. Appl. Phys.* **117**, 17A740 (may 2015).

[8] Thomson, W., [*Theory of vibration with applications*], CRC Press (1996).

[9] Gross, D., Hauger, W., Schrder, J., and Wall, W. A., [*Technische Mechanik 2*], Springer Berlin Heidelberg (2012).

[10] Hoffmann, R. and Wolff, M., [*Intelligente Signalverarbeitung 1*], Springer Science + Business Media (2014).

[11] Marschner, U., Gerlach, G., Starke, E., and Lenk, A., "Equivalent circuit models of two-layer flexure beams with excitation by temperature, humidity, pressure, piezoelectric or piezomagnetic interactions," *Journal of Sensors and Sensor Systems* **3**, 187–211 (sep 2014).

[12] Joule, J., "On a new class of magnetic forces," *Ann. Electr. Magn. Chem* **8**(1842), 219–224 (1842).

[13] Marschner, U., Datta, S., Starke, E., Pfeifer, G., Fischer, W.-J., and Flatau, A. B., "Magnetostrictive unimorph transducer network model," in [*Sensors and Smart Structures Technologies for Civil, Mechanical, and Aerospace Systems 2010*], Tomizuka, M., ed., SPIE-Intl Soc Optical Eng (mar 2010).

[14] Freymann, R., "Balkentheorie," in [*Strukturdynamik*], 75–106, Springer Science + Business Media (2011).

[15] Johnson, D., "Origins of the equivalent circuit concept: The voltage-source equivalent," *Proceedings of the IEEE* **91**, 636–640 (apr 2003).

[16] Petrascheck, D. and Schwabl, F., [*Elektrodynamik*], Springer Science + Business Media (2016).

[17] Wolschin, G., "Magnetostatik," in [*Elektrodynamik*], 69–87, Springer Science + Business Media (2016).

[18] Deng, Z. and Dapino, M. J., "Modeling and design of galfenol unimorph energy harvesters," *Smart Mater. Struct.* **24**, 125019 (nov 2015).

[19] Germer, M., Marschner, U., J.H.Yoo, and Flatau, A., "Equivalent eletromechanical circuit analysis for electrical tunning of magnetostrictive unimorph system dynamics," in [*ASME 2016 Conference on Smart Materials, Adaptive Structures and Intelligent Systems, Volume 1*], ASME International (2016).

[20] INC., K. M., "http://www.kjmagnetics.com/ (10-02-2016)."

[21] Yoo, J.-H. and Flatau, A. B., "Measurement of field-dependence elastic modulus of iron–gallium alloy using tensile test," *J. Appl. Phys.* **97**(10), 10M318 (2005).